







Article

Synthesis, Characterization, and Biological Properties of Iron Oxide Nanoparticles Synthesized from *Apis mellifera* Honey

Hamna Shahid ¹, Aqeel Ahmed Shah ², Syed Nizam Uddin Shah Bukhari ³, Anjum Zehra Naqvi ⁴, Iqra Arooj ^{1,*}, Mehvish Javeed ¹, Muhammad Aslam ⁵, Ali Dad Chandio ², Muhammad Farooq ⁶, Sadaf Jamal Gilani ⁷ and May Nasser Bin Jumah ^{8,9,10}

- ¹ Department of Microbiology & Molecular Genetics, Faculty of Life Sciences, The Women University, Multan 66000, Pakistan; hamnashahid185@gmail.com (H.S.); mehvish.mmg23@wum.edu.pk (M.J.)
- ² Wet Chemistry Laboratory, Department of Metallurgical Engineering, NED University of Engineering and Technology, University Road, Karachi 75270, Pakistan; aqeelshah@cloud.neduet.edu.pk (A.A.S.); alidad@neduet.edu.pk (A.D.C.)
- ³ Department of Basic Science and Humanities, Dawood University of Engineering and Technology, Karachi 74800, Pakistan; nizamuddin@duet.edu.pk
- ⁴ Department of Microbiology, University of Karachi, Karachi 75270, Pakistan; aznaqvi@uok.edu.pk
- ⁵ Institute of Physics and Technology, Ural Federal University, Mira Str. 19, 620002 Yekaterinburg, Russia; aslam@urfu.ru
- ⁶ Pakistan Council of Scientific and Industrial Research (PCSIR), PCSIR Head Office, 01-Constitution Avenue, Sector G-5/2, Islamabad 44000, Pakistan; mfaruq752@gmail.com
- ⁷ Department of Basic Health Sciences, Foundation Year, Princess Nourah bint Abdulrahman University, Riyadh 11671, Saudi Arabia; sjglani@pnu.edu.sa
- ⁸ Biology Department, College of Science, Princess Nourah bint Abdulrahman University, Riyadh 11671, Saudi Arabia; mnbinjumah@pnu.edu.sa
- ⁹ Environment and Biomaterial Unit, Health Sciences Research Center, Princess Nourah bint Abdulrahman University, Riyadh 11671, Saudi Arabia
- ¹⁰ Saudi Society for Applied Science, Princess Nourah bint Abdulrahman University, Riyadh 11671, Saudi Arabia
- * Correspondence: iqra.6051@wum.edu.pk



Citation: Shahid, H.; Shah, A.A.; Shah Bukhari, S.N.U.; Naqvi, A.Z.; Arooj, I.; Javeed, M.; Aslam, M.; Chandio, A.D.; Farooq, M.; Gilani, S.J.; et al. Synthesis, Characterization, and Biological Properties of Iron Oxide Nanoparticles Synthesized from *Apis mellifera* Honey. *Molecules* **2023**, *28*, 6504. <https://doi.org/10.3390/molecules28186504>

Academic Editor: Hwei Voon Lee

Received: 9 June 2023

Revised: 28 August 2023

Accepted: 5 September 2023

Published: 7 September 2023



Copyright: © 2023 by the authors. Licensee MDPI, Basel, Switzerland. This article is an open access article distributed under the terms and conditions of the Creative Commons Attribution (CC BY) license (<https://creativecommons.org/licenses/by/4.0/>).

Abstract: Green approaches for nanoparticle synthesis have emerged as biocompatible, economical, and environment-friendly alternatives to counteract the menace of microbial drug resistance. Recently, the utilization of honey as a green source to synthesize Fe₂O₃-NPs has been introduced, but its antibacterial activity against one of the opportunistic MDR pathogens, *Klebsiella pneumoniae*, has not been explored. Therefore, this study employed *Apis mellifera* honey as a reducing and capping agent for the synthesis of iron oxide nanoparticles (Fe₂O₃-NPs). Subsequent to the characterization of nanoparticles, their antibacterial, antioxidant, and anti-inflammatory properties were appraised. In UV-Vis spectroscopic analysis, the absorption band ascribed to the SPR peak was observed at 350 nm. XRD analysis confirmed the crystalline nature of Fe₂O₃-NPs, and the crystal size was deduced to be 36.2 nm. Elemental analysis by EDX validated the presence of iron coupled with oxygen in the nanoparticle composition. In ICP-MS, the highest concentration was of iron (87.15 ppm), followed by sodium (1.49 ppm) and other trace elements (<1 ppm). VSM analysis revealed weak magnetic properties of Fe₂O₃-NPs. Morphological properties of Fe₂O₃-NPs revealed by SEM demonstrated that their average size range was 100–150 nm with a non-uniform spherical shape. The antibacterial activity of Fe₂O₃-NPs was ascertained against 30 clinical isolates of *Klebsiella pneumoniae*, with the largest inhibition zone recorded being 10 mm. The MIC value for Fe₂O₃-NPs was 30 µg/mL. However, when mingled with three selected antibiotics, Fe₂O₃-NPs did not affect any antibacterial activity. Momentous antioxidant (IC₅₀ = 22 µg/mL) and anti-inflammatory (IC₅₀ = 70 µg/mL) activities of Fe₂O₃-NPs were discerned in comparison with the standard at various concentrations. Consequently, honey-mediated Fe₂O₃-NP synthesis may serve as a substitute for orthodox antimicrobial drugs and may be explored for prospective biomedical applications.

Keywords: green synthesis; honey mediation; Fe₂O₃-NPs; antibacterial activity

1. Introduction

Nanotechnology has attracted immense attention during the last two decades owing to its diverse applications in various fields of science. The versatility of nanoparticles is particularly evident due to their small size, which is usually less than 100 nm [1,2]. A reduction in size determines several features of nanoparticles, including enhanced surface area and improved magnetic and electrochemical properties [3]. Organic product synthesis with nanotechnology is an evolving area because nanotechnology offers numerous benefits in the natural delivery of drugs to heal chronic illnesses [4]. Metal oxide nanoparticles are being studied frequently nowadays due to their unique features [5]. Magnetic nanoparticles of metals, particularly iron oxide nanoparticles (Fe₂O₃-NPs), with validated biological strength and biocompatibility, are the focus of applications, including drug delivery, magnetic resonance imaging, and bioremediation [6–8]. Hematite (Fe₂O₃), magnetite (Fe₃O₄), and limonite (Fe₂O₃ · H₂O) are the most common forms of iron oxides [9,10]. Fe₂O₃-NPs can be synthesized by using chemical methods such as microemulsions, co-precipitation of Fe²⁺ ions, the sol–gel method, sonochemistry, the colloidal method, non-aqueous routes, the pyrolysis reaction, and emulsion techniques [11–14]. These methods produce harmful chemicals. So, there has been an expanding incentive to use microorganisms and green approaches in Fe₂O₃-NP synthesis [15].

A recent study reported the successful synthesis of Fe₂O₃-NPs by using aqueous extracts of *Azadirachta indica* [16]. Similarly, other recent studies have reported the synthesis of Fe₂O₃-NPs from aqueous extracts of *Ficus carica* and *Hylocereus undantus* [3,16,17]. Various sugars, terpenoids, polyphenols, alkaloids, phenolic acids, and proteins are commonly found in natural extracts and account for their reducing and capping abilities, resulting in stable maintenance of the nanoparticle structure. It has been proven that functional groups such as C–O–C, C–O, C=C, and C=O present in these compounds can markedly assist nanoparticle synthesis [18,19]. *Apis mellifera* honey has been used since ancient times for its therapeutic value [20]. Honey is a natural organic source of nutrition that contains a large amount of glucose and fructose (75%) that act as reducing and stabilizing agents in nanoparticle synthesis [21]. Honey-mediated nanoparticle synthesis does not produce any hazardous by-products that are harmful to human health when used in medical applications. Additionally, honey-mediated green synthesis is a biocompatible, quick, and easy approach that may be utilized to produce a wide range of beneficial end-products in diverse applications [22]. In the past few years, several studies have surfaced on the successful synthesis of biogenic Fe₂O₃-NPs [4].

Recently, researchers reported significant in vitro antibacterial potential of honey-loaded Fe₂O₃ nanoparticles against *P. aeruginosa*, *B. subtilis*, *S. aureus*, *E. coli*, *Penicillium* spp., and *Aspergillus* spp. [23]. Another study reported the successful synthesis of Fe₂O₃-NPs from *Oscillatoria limnetica*. Researchers reported significant antibacterial activities of Fe₂O₃-NPs against MDR *E. coli*, *S. aureus*, and *B. subtilis* [24]. Likewise, Fe₂O₃-NPs were produced effectively by utilizing gum extract from *Bombax malabaricum*. It was discovered that the bioactive compounds and phytochemicals included in the gum extract of *B. malabaricum* were responsible for the creation of Fe₂O₃-NPs. In that study, the antibacterial activity of synthesized NPs was studied against *S. aureus*, *B. halodurans*, and *M. luteus* with significant results [25]. The antibacterial potential of Fe₂O₃-NPs is of particular relevance in present times because the spread of antibiotic-resistant species has become a key problem for global health [10]. Fe₂O₃-NPs have been proven to be effective against a variety of infectious microorganisms due to their ability to generate highly reactive oxygen species [26]. It is hypothesized that the antimicrobial effect of Fe₂O₃-NPs is mainly related to their morphological and physiological characteristics [27].

Klebsiella pneumoniae is a proactive pathogen that causes an array of diseases in immunodeficient individuals, such as diabetic patients, neonates, and cancer patients [28]. Multidrug resistance and the emergence of hypervirulent strains of *K. pneumoniae* have been reported and are responsible for a 42% mortality rate in patients and healthy individuals [29]. However, to the best of our knowledge, the in vitro antibacterial potential of Fe_2O_3 -NPs, specifically against the clinical isolates of *K. pneumoniae*, has not been assessed before. Hence, in this research, pure honey was utilized as a reducing and stabilizing agent to produce Fe_2O_3 -NPs by using iron chloride hexahydrate ($\text{FeCl}_3 \cdot 6\text{H}_2\text{O}$) and sodium hydroxide. Further, the characterization of biogenic nanoparticles was performed using numerous techniques, and their antibacterial, antioxidant, and anti-inflammatory potentials were evaluated.

2. Results

2.1. Visual Observation and UV-Vis Spectroscopy

A. mellifera honey was recognized as a good source for the synthesis of Fe_2O_3 -NPs. In the present study, the production of Fe_2O_3 -NPs started when NaOH was gradually added with stirring to a primary solution containing iron salt and sodium hydroxide. The development of an intense black color provided a visual indication of the presence of nanoparticles in the solution (Figure 1). Primary confirmation was carried out with the help of UV-Vis spectroscopic analysis, which showed a sharp peak at 350 nm, confirming the surface plasmon resonance of the synthesized Fe_2O_3 -NPs (Figure 2a).

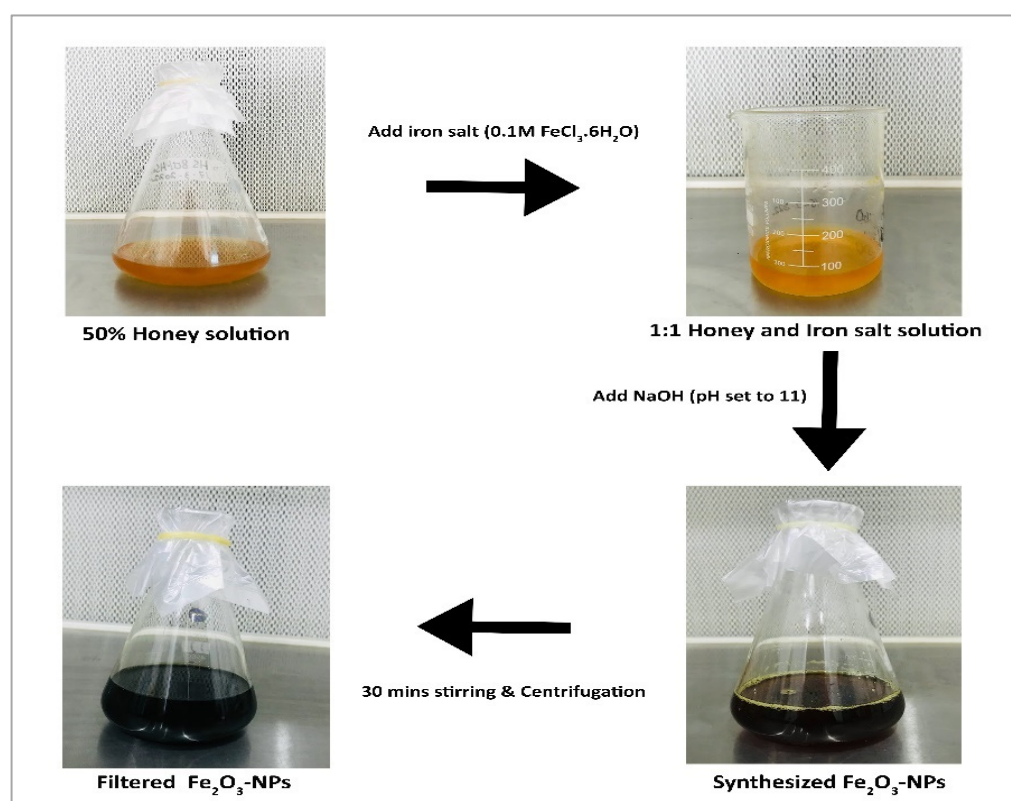


Figure 1. Visual observation of color change from yellow to intense black during synthesis of Fe_2O_3 -NPs.

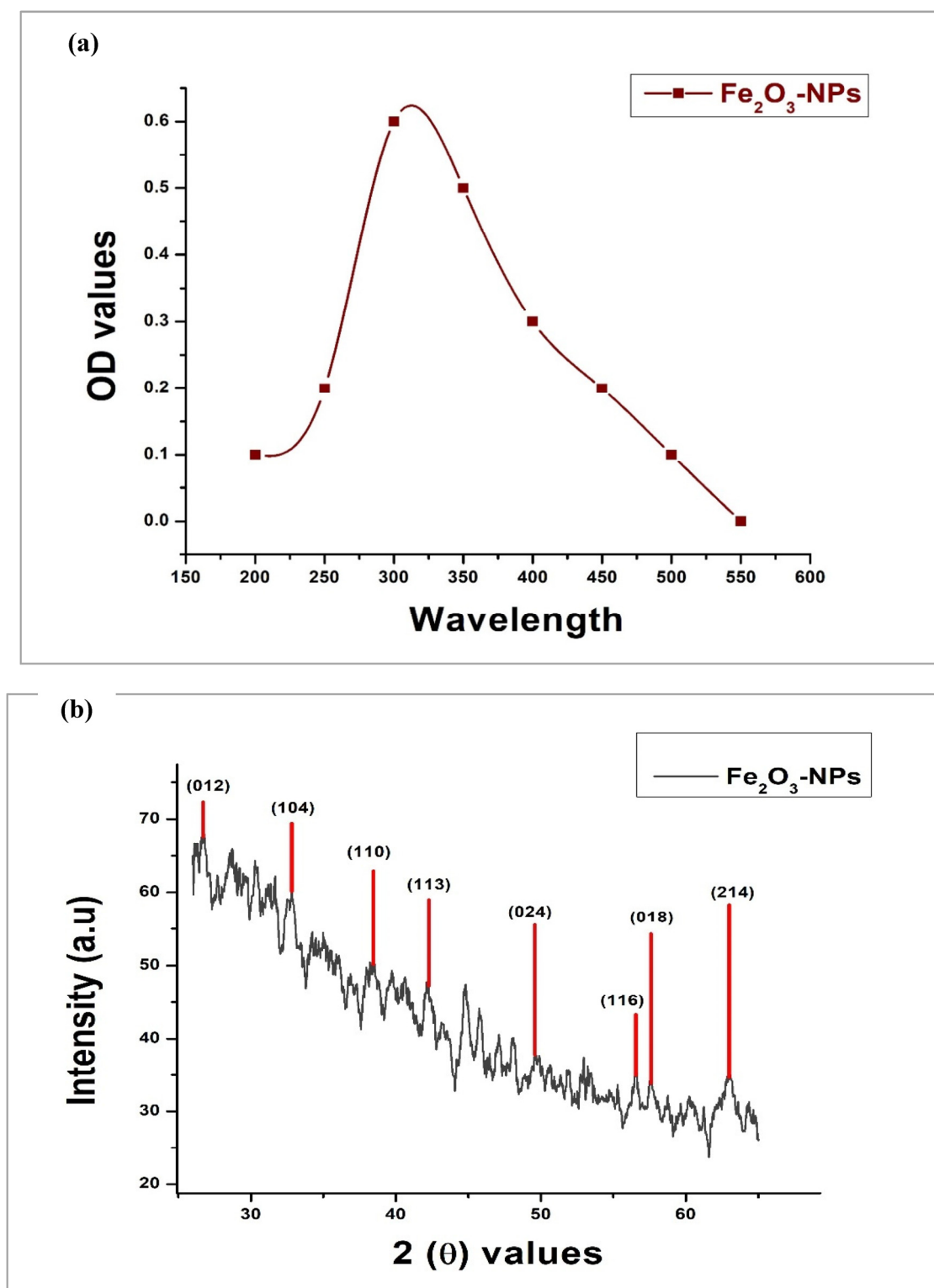


Figure 2. Cont.

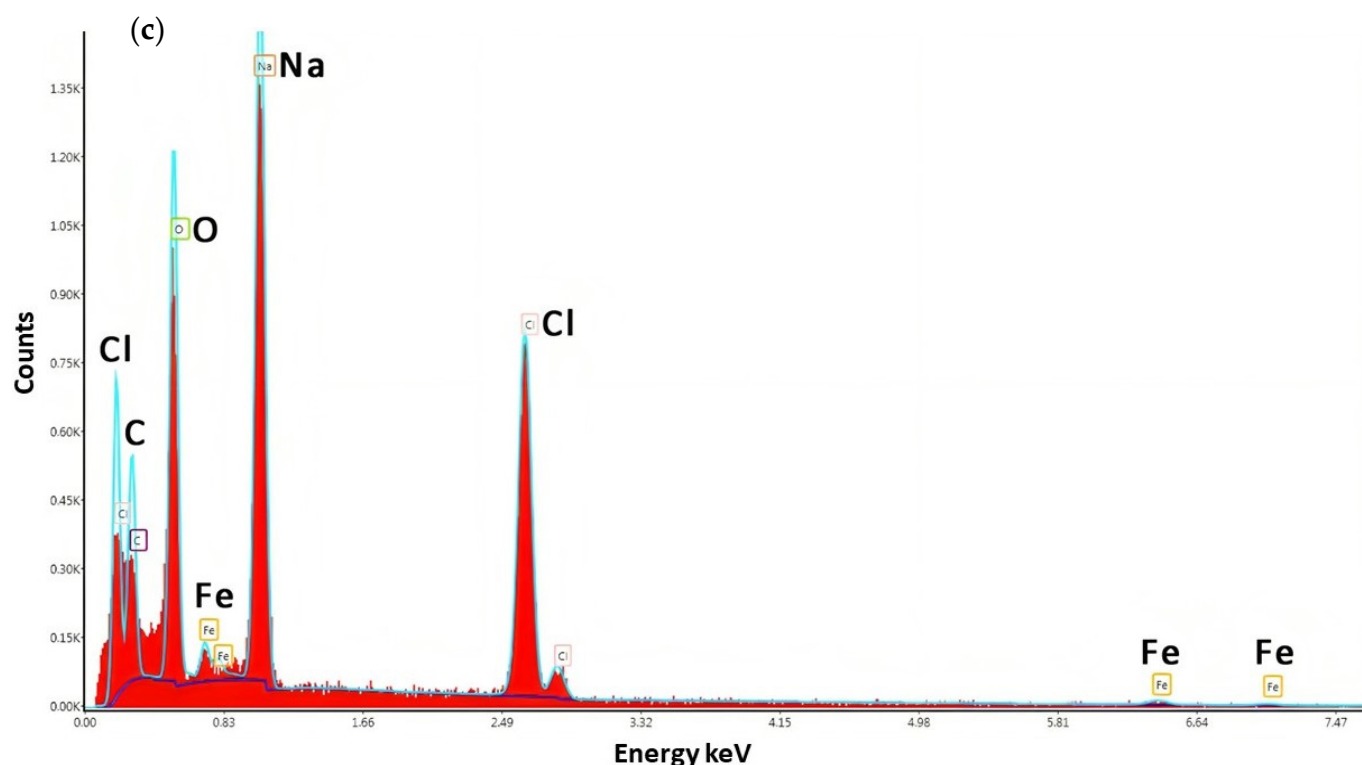


Figure 2. Results representing the characterization of biogenic Fe_2O_3 -NPs. (a) UV-visible graph (a sharp peak at 350 nm is attributed to Fe_2O_3 -NPs); (b) XRD graph (highlighted peaks are attributed to crystalline nature of Fe_2O_3 -NPs); (c) EDX graph (clear Fe and O peaks).

2.2. Characterization by XRD, EDX, ICP-MS, VSM, and SEM

In order to determine the single phase and crystalline nature of nanoparticles, XRD analysis was carried out. As represented in Figure 2b, intense peaks at 2θ values of 24.68° , 33.88° , 38.44° , 41.36° , 49.8° , 56.64° , 57.48° , and 62.88° corresponding to index values of (012), (104), (110), (113), (024), (116), (018), and (214) were observed for Fe_2O_3 -NPs. These values were contrasted with those of the Joint Committee on Powder Diffraction Standards (JCPDS No. 24-0072) for Fe_2O_3 -NPs. These crystal planes clearly represent the crystalline nature of Fe_2O_3 -NPs in the sample, and the average crystal size was measured as 36.2 nm by using the Debye–Scherer equation ($D = K \lambda / \beta 1 / 2 \cos \theta$) with an average lattice strain of 0.00285. These crystal planes indicated that synthesized Fe_2O_3 -NPs may be in a rhombohedral crystal phase with lattice constants of $a = b = 5.0346 \text{ \AA}$ and $c = 13.7473 \text{ \AA}$. These lattice constant parameters were matched with the Crystallography Open Database (COD No. 9015964).

The EDX analysis shown in Figure 2c revealed the elemental composition of the synthesized Fe_2O_3 -NP solution. K- α peaks between 0.0 and 0.83 keV confirmed that Fe and O are present in the synthesized nanoparticles. The abundance of oxygen demonstrated that the nanoparticles are in iron oxide form. Peaks of C and O atoms confirmed the contribution of honey in the synthesis of nanoparticles. The presence of Na and Cl atoms was also detected as impurities in the solution. In the present study, the highest proportion of Fe elements was found in the EDX spectra, indicating that the main component was Fe_2O_3 -NPs (Table 1).

Table 1. The elemental composition of synthesized Fe_2O_3 -NPs as per the EDX analysis.

Element	Weight %	Atomic %	Net Int.
Fe O	40.73	50.48	363.77
Na Cl	7.58	4.87	40.73

ICP-MS analysis was performed to determine the trace element concentration in the synthesized Fe_2O_3 -NPs. The concentration of each trace element was determined in ppm (parts per million) at different wavelengths. According to the results, Fe was found to be at its highest concentration of 87.15 ppm at a wavelength of 238.204 nm with an intensity of 762,552.31 counts per second (c/s), while a 1.49 ppm concentration was measured for Na, which was found at 589.590 nm with an intensity of 508.64 c/s (Table 2).

Table 2. The trace element composition of synthesized Fe_2O_3 -NPs as per the ICP-MS analysis.

Trace Elements	Wavelength (nm)	Concentration (ppm)
Fe	238.204	87.15
Na	589.590	1.49
As	188.980	0.02
Cd	214.439	0.09
Co	238.892	0.03
Cr	267.716	0.02
Cu	327.395	−0.03
Mg	279.553	0.02
Mn	257.610	0.02
Ni	231.604	0.07
Pb	220.353	0.06
Zn	213.857	0.02
Se	196.026	0.02

Figure 3 shows the magnetic hysteresis loop (MH-loop) for synthesized hematite Fe_2O_3 -NPs at 299 K. The curve revealed the weak ferromagnetic behavior of the synthesized Fe_2O_3 -NPs with a saturation magnetization (M_s) value of 0.336 e.m.u./g at 1 Tesla (10,000 Oe). The morphological (size and shape) properties of the produced Fe_2O_3 -NPs, as determined by SEM, are depicted in Figure 4. These images confirmed the development of nanostructures, which were well distributed in the solution. A continuous variation was observed in the shape and size of the produced Fe_2O_3 -NPs. At 19,000x magnification, the size distribution of Fe_2O_3 -NPs was estimated to be in the range of 100–200 nm with a non-uniform spherical shape.

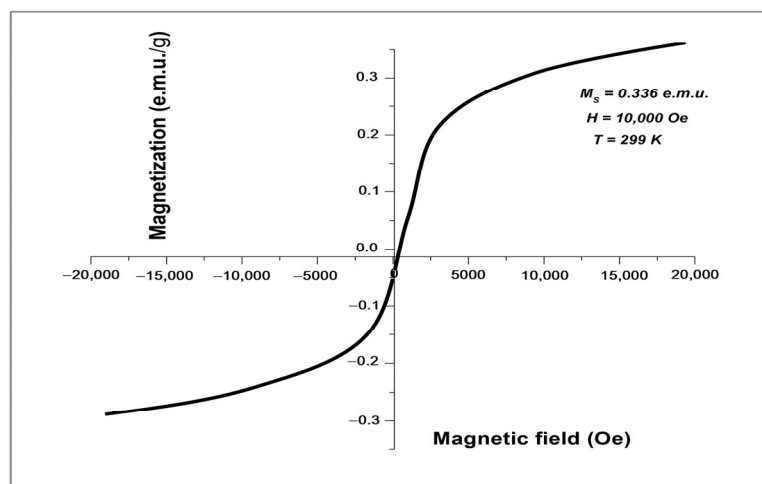


Figure 3. Magnetic behavior of Fe_2O_3 -NPs as measured by vibrating sample magnetometry.

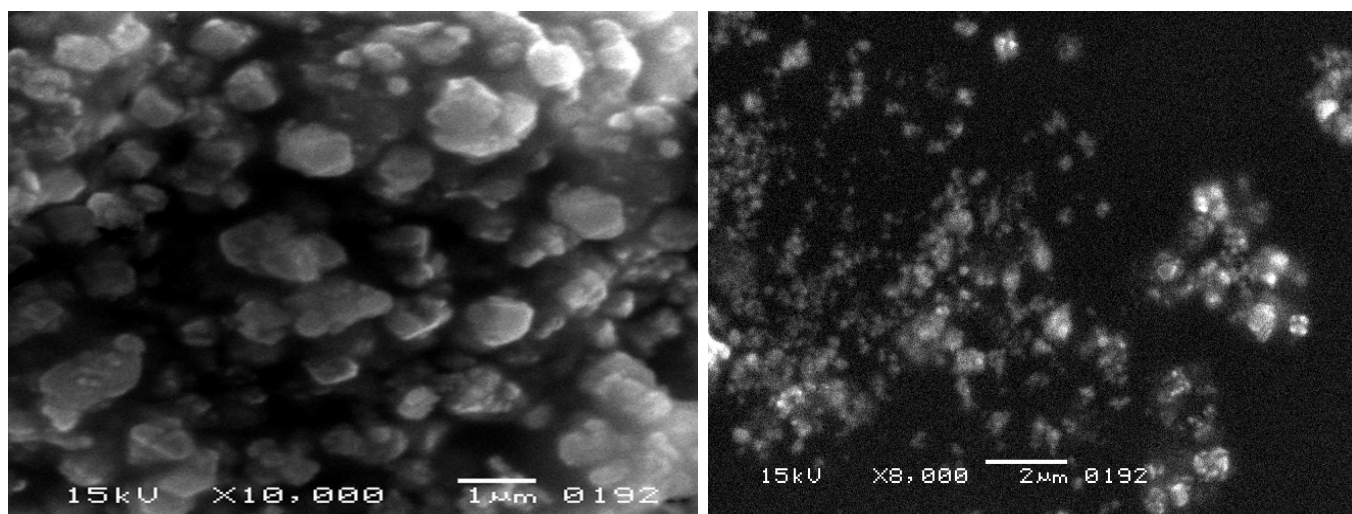


Figure 4. SEM images of Fe_2O_3 -NPs at magnification up to 10,000x.

2.3. Antibacterial Studies

In the present research, the antibacterial activity of newly synthesized Fe_2O_3 -NPs was studied in detail against one of the notorious opportunistic Gram-negative bacteria, *K. pneumoniae*. A 30 $\mu\text{g}/\text{mL}$ concentration of Fe_2O_3 -NPs revealed the most significant in vitro antibacterial property against all isolates of *K. pneumoniae*, as demonstrated by the measured zone diameters (Figure 5a). However, the honey solution did not show any bactericidal effect when used alone, as no zones of inhibition could be observed (Figure 5b). Among all isolates, the largest inhibition zone of 10 mm was observed against HS-K4, HS-K-5, HS-K9, and HS-K-15. On the other hand, the lowest inhibition zone of 5 mm was recorded against HS-K-17 and HS-K-19. Intermediate values of 6 mm to 9 mm were observed against the other 24 isolates of *K. pneumoniae*.

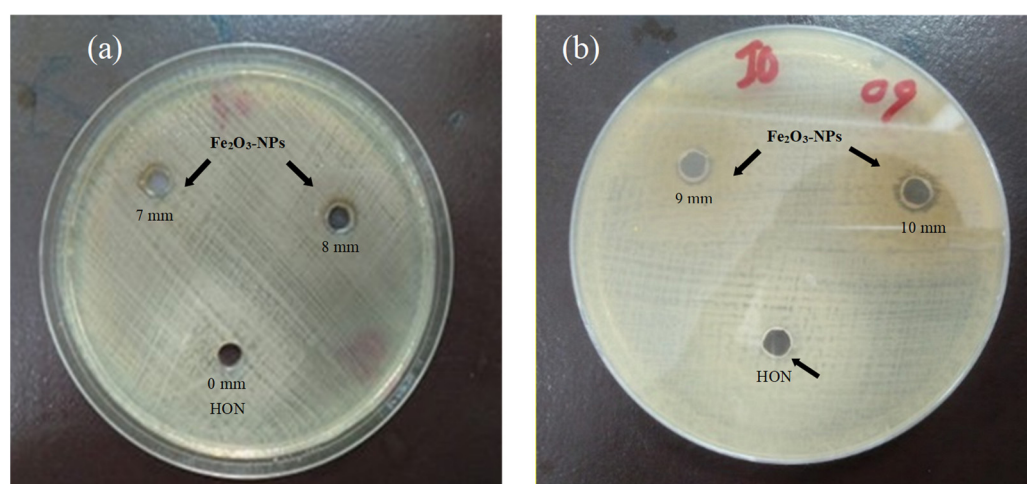


Figure 5. Antibacterial potential of Fe_2O_3 -NPs. (a,b) MH agar plates display the antibacterial property of Fe_2O_3 -NPs against *K. pneumoniae*; (b) arrow is pointing towards the minimal antibacterial effect of honey in comparison with Fe_2O_3 -NPs against *K. pneumoniae*.

The MIC value for synthesized Fe_2O_3 -NPs against *K. pneumoniae* was interpreted as 30 $\mu\text{g}/\text{mL}$ based on ELISA reader absorbance values. After incubation, the in vitro efficacy of antibiotics was examined against clinical strains of *K. pneumoniae*. The antibacterial activity of nanoparticles was also measured in combination with three selected antibiotics and compared with the individual antibacterial potential of nanoparticles and antibiotics.

The results were equated to CLSI guidelines and interpreted as follows: all strains of *K. pneumoniae* showed an intermediate resistant (I) pattern against CN-10 and FEP-30, while all strains showed sensitivity (S) to CIP-5. Surprisingly, when antibiotics and nanoparticles were used in combination, no zones of inhibition could be seen at all.

2.4. Antioxidant Potential

The antioxidant potential of Fe_2O_3 -NPs was found to be superior to that of the standard. At concentrations of 200, 400, 600, and 800 $\mu\text{g/mL}$, absorbance values of 1.65, 1.97, 2.16, and 2.24 were measured for Fe_2O_3 -NPs, respectively. At the same concentrations of AAE, which were included as a standard, absorbance values of 2.2, 2.35, 2.51, and 2.66 were recorded, respectively. The absorption readings for HON at the concentrations of 200 $\mu\text{g/mL}$, 400 $\mu\text{g/mL}$, 600 $\mu\text{g/mL}$, and 800 $\mu\text{g/mL}$ were 2.13, 2.2, 2.38, and 2.45, respectively. Figure 6a represents the IC_{50} value in terms of total antioxidant capacity (TAC), and it was calculated to be 22 $\mu\text{g/mL}$ for Fe_2O_3 -NPs. Furthermore, it was interpreted from the graph included in Figure 6b that the antioxidant capacity of nanoparticles correspondingly increased with an increase in their concentration in the sample.

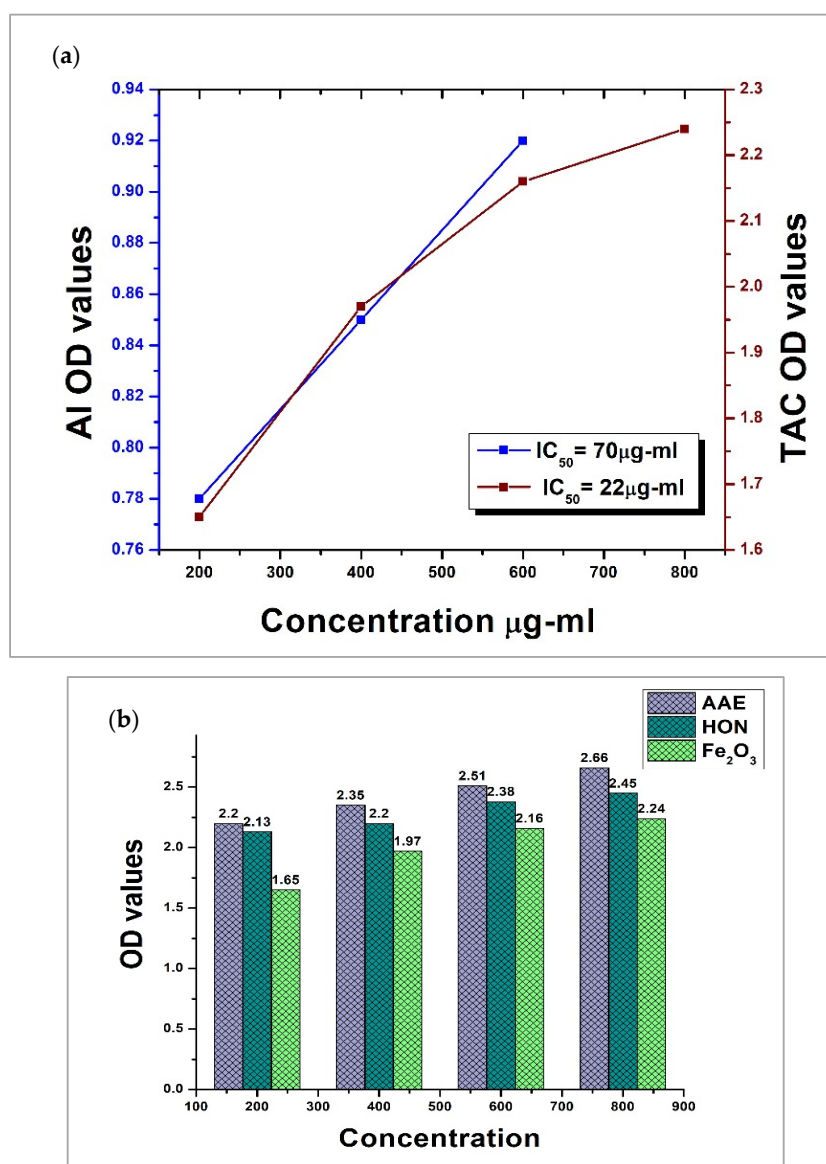


Figure 6. Cont.

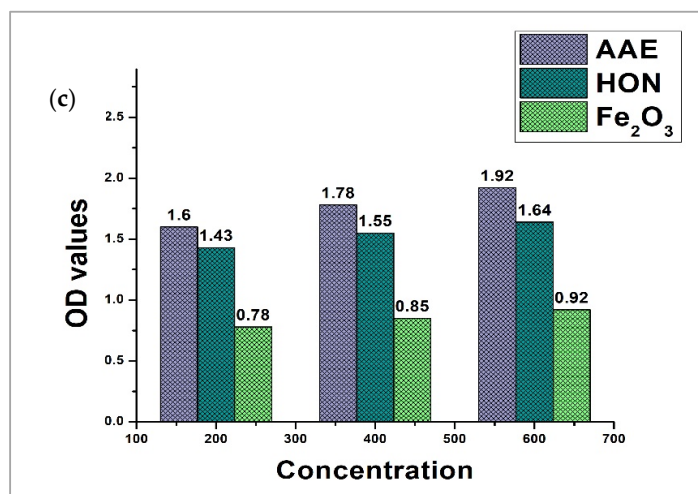


Figure 6. Antioxidant and anti-inflammatory potential of Fe₂O₃-NPs. (a) IC₅₀ values for total antioxidant capacity (TAC) and anti-inflammatory (AI) activity of Fe₂O₃-NPs in terms of ascorbic acid (AAE) and honey (HON); (b) TAC values for different concentrations of Fe₂O₃-NPs in terms of AAE and HON; (c) AI values for different concentrations of Fe₂O₃-NPs in terms of AAE and HON.

2.5. Anti-Inflammatory Potential

Honey-mediated Fe₂O₃-NPs manifested considerably greater anti-inflammatory potential as compared to the standard. Absorbance values of 0.78, 0.85, and 0.92 were measured for the synthesized nanoparticles at different concentrations of 200, 400, and 600 µg/mL, respectively. On the contrary, at the same concentrations, AAE was demonstrated to possess absorbance values of 1.6, 1.78, and 1.92, respectively, whereas the spectrophotometer readings for HON at concentrations of 200 µg/mL, 400 µg/mL, and 600 µg/mL were 1.43, 1.55, and 1.64, respectively. Figure 6a illustrates the IC₅₀ value for Fe₂O₃-NPs in terms of anti-inflammatory potential (AI), and it was calculated to be 70 µg/mL. From the graph shown in Figure 6c, it was deduced that anti-inflammatory capacity increased as the concentration of Fe₂O₃-NPs increased in the solution.

3. Discussion

Fabrication of Fe₂O₃-NPs utilizing the capping and stabilizing agents in biological resources is a biocompatible, eco-friendly, and nontoxic approach with widespread biomedical applications. Recently, these nanoparticles have drawn considerable attention owing to the magnetic properties and flexible surface chemistry of iron oxide [30]. The utilization of honey as a single antecedent in the production of Fe₂O₃-NPs produced results that are equivalent to those achieved when using only glucose or fructose. Since honey exhibits an analogous pattern with respect to the size of particle decline during Fe₂O₃-NP creation [31], in this study, *Apis mellifera* honey-loaded Fe₂O₃-NPs were synthesized and evaluated for their potential biological properties. During synthesis, the appearance of an intense black color provided a visual indication of the successful synthesis of nanostructures. Previous studies have also reported the formation of an intense black color toward the end of the synthesis procedure for Fe₂O₃-NPs [7,15,26].

In the present study, Fe₂O₃-NPs were characterized in more detail using UV-Vis analysis, which can be utilized to learn essential details about Fe₂O₃-NPs' sturdiness, size, and shape [32]. A clear and intense peak was observed at 350 nm, which corresponded to the presence of Fe₂O₃-NPs in the sample. Similar results were described in a previous study that reported the green synthesis of Fe₂O₃-NPs [4]. The crystalline structure of biogenic Fe₂O₃-NPs was evaluated using XRD analysis. Sharp diffraction peaks were observed at various index values ((012), (104), (110), (113), (024), (116), (018), and (214)), which revealed that the synthesized nanoparticles possessed extremely fine nature, a good crystalline rhombohedral structure, and a calculated size of 36.2 nm ($a = b = 5.0346 \text{ \AA}$,

$c = 13.7473 \text{ \AA}$). This was in line with previous observations regarding nanoparticle crystal size [33]. Previous studies reported the similar crystal planes of (012), (104), (110), (113), (024), (116), (018), and (214) at similar 2θ values for Fe_2O_3 -NPs that can be correlated with the current study [26,34].

EDX analysis was used to determine the elemental content of the sample. Iron typically exhibits an intense peak at 0.7–7 keV [35]. The EDX graph clearly depicts the presence of one K- α peak before 0.8 keV, which can be attributed to iron atoms, and two K- α peaks between 0.0 keV and 0.83 keV, which can be ascribed to carbon and oxygen atoms. The presence of carbon and oxygen, together with iron, confirmed the involvement of honey in the synthesis of nanoparticle structures. This led to the production of quantitative as well as qualitative evaluations of the iron components that contributed to the generation of Fe_2O_3 -NPs [36]. Cl and Na atoms were also found as residual impurities while synthesizing nanoparticles from ferric chloride, and this has been documented in previous studies [37]. Several earlier studies that performed XRD and EDX analyses of Fe_2O_3 -NPs synthesized from different natural sources reported similar observations [38,39]. Furthermore, the ICP-MS technique was used to measure the exact concentration of elements (Fe and Na) in synthesized nanoparticles. The measured concentrations of Fe and Na were 87.15 ppm (238.204 nm) and 1.49 ppm (589.590 nm), respectively. These results confirmed the presence of Fe atoms, which dominated others in synthesized nanoparticles, pointing towards the highest proportion of Fe_2O_3 -NPs in the sample. Another study reported a concentration of ultra-filtered Fe_2O_3 -NPs in suspension, which was in line with our observations [40].

The MH-loop produced by VSM analysis confirmed that the synthesized Fe_2O_3 -NPs had weak ferromagnetic properties. The M_s value of 0.336 e.m.u. can be correlated to Fe_2O_3 -NPs with bulk hematite, as reported in an earlier study [41]. Some previous studies reported superparamagnetic properties of small-sized (<90 nm) hematite Fe_2O_3 -NPs with calculated M_s values of 8.5 e.m.u./g and 0.96 e.m.u./g at 300 K [42,43]. A previous study reported the anti-ferromagnetic (non-saturating magnetization) properties of hematite Fe_2O_3 -NPs even at a temperature of 1000 K [44]. The SEM images with a magnification of up to 20,000x revealed that the nanoparticle size distribution was in the range of 100 nm and 200 nm. Recent studies have also demonstrated that the size of iron oxide-based nanoparticles is between 10 nm and 100 nm [45,46]. In the present study, the shape of Fe_2O_3 -NPs was estimated to be irregularly spherical. A previous study also reported a cavity-like shape with a rough surface of Fe_2O_3 -NPs [47]. The SEM images of the present study revealed that the precursor (honey) was stabilizing the surface of nanoparticles by selectively slowing their growth rate and stopping particle aggregation. This result can be correlated with a previous similar study [23]. Another study demonstrated that the nature of Fe_2O_3 -NPs was not uniform and that they were present mostly in the form of large, agglomerated groups. These clusters were linked to the low capping ability of the plant source and the magnetic properties of Fe_2O_3 -NPs [26].

The antimicrobial activity of honey-mediated Fe_2O_3 -NPs was evaluated against clinical strains of *K. pneumoniae*, and significant antibacterial activity was observed against all strains of *K. pneumoniae*. The estimated MIC value for the formulated nanoparticles was 30 $\mu\text{g/mL}$. Significant antibacterial activity of Fe_2O_3 -NPs synthesized from different organic extracts has been reported previously against various groups of bacteria, including *Pseudomonas* spp., *E. coli*, *S. aureus*, and *B. cereus*, among others [47,48]. A recent study also reported a 10 mm inhibition zone as the highest for Fe_2O_3 -NPs against *S. aureus* [23]. In line with these findings, the authors noticed that if the concentration of nanoparticles in the solution increased, the antibacterial properties improved. Many studies have been conducted to elucidate the mechanisms, and it has been determined that the antimicrobial activity of nanoparticles is largely dependent on capping agents [49,50]. Several scientists have also found that relatively smaller nanoparticles display better antibacterial potential [51,52]. Although it is still unclear how exactly metal or metal oxide NPs work to kill bacteria, Fe_2O_3 -NPs work by blocking cellular proteins and enzymes from replicating. According to much research, nanoparticles damage the integrity of cells by penetrating both the cell wall

and the membrane, as well as by triggering the death of cells by damaging nucleic acids and proteins [25].

In the present study, no synergistic potential of the synthesized nanoparticles with antibiotics was observed because no zones of inhibition were recorded on the MH agar plates subsequent to the incubation time period. On the contrary, Abo-Shama et al. (2020) and some others have reported good synergistic activity between various metallic nanomaterials and different commercially available antibiotics [53]. In our study, the lack of synergism could be due to the high concentration of honey in the solution, which blocked the diffusion of antibiotics into the agar, or poor chemical compatibility between fabricated nanoparticles and antibiotics. The second hypothesis seems closer to reality, as the antibacterial effect of nanoparticles was missing in the presence of antibiotics. Hence, it can be safely concluded that honey-mediated Fe_2O_3 -NPs and antibiotics suppressed each other's antibacterial effects.

The antioxidant potential of different aqueous samples of formulated nanoparticles was measured using the TAC method. The results illustrated the significant antioxidant capacity of all nanoparticle concentrations ($200\ \mu\text{g/mL} = 1.65\ \text{OD}$, $400\ \mu\text{g/mL} = 1.97\ \text{OD}$, $600\ \mu\text{g/mL} = 2.16\ \text{OD}$, and $800\ \mu\text{g/mL} = 2.24\ \text{OD}$), which was approximately equal to that of HON and less than that of standard AAE. After incubation, a very dark blue hue was noticed in the test tubes, which was similar to the control. The IC_{50} value for newly synthesized nanoparticles was estimated at $22\ \mu\text{g/mL}$ in terms of TAC. In the present study, a 50% honey solution was used to produce nanoparticles, and due to the high concentration of honey in the final solution, a very strong antioxidant potential was seen with a very low IC_{50} value. Recently, the good antioxidant potential of nanoparticles based on iron oxide resulting from distinctive biological resources has been observed with significant IC_{50} values ($20.456\ \mu\text{g/mL}$, $58.85\ \text{mg/mL}$, $45.4\ \text{mg/mL}$, $33\ \text{mg/mL}$) [54–56].

The anti-inflammatory activity of our synthesized nanoparticles was determined in terms of BSA using the protein inhibition method. Various aqueous concentrations of newly synthesized Fe_2O_3 -NPs revealed better anti-inflammatory activities ($200\ \mu\text{g/mL} = 0.78\ \text{OD}$, $400\ \mu\text{g/mL} = 0.85\ \text{OD}$, $600\ \mu\text{g/mL} = 0.92\ \text{OD}$) in comparison with AAE or HON, and their IC_{50} value was measured at $70\ \mu\text{g/mL}$. A recent study reported significant anti-inflammatory activity of nano-ointment that was fabricated with iron oxide and zinc oxide nanoparticles [57]. Another study reported the significant percentage inhibition of Fe_2O_3 -NPs at different concentrations ($100 = 25.68\%$, $200 = 45.43\%$, $300 = 60.59\%$, $400 = 82.49\%$, $500 = 92.59\%$, IC_{50} value = $234.45\ \mu\text{g/mL}$). The anti-inflammatory activity of these Fe_2O_3 -NPs revealed their protective nature. It is a common occurrence for secondary or tertiary protein structures to disintegrate, leading to a disruption of biological function [2]. Therefore, it can be stated that honey-mediated synthesis of Fe_2O_3 -NPs leads to reliable antibacterial, antioxidant, and anti-inflammatory effects, which can be pursued in future studies.

4. Materials and Methods

4.1. Honey-Mediated Synthesis of Fe_2O_3 -NPs

Organic honey of *Apis mellifera* (honeybee) was bought from the local market in Multan, Pakistan. For green synthesis, 50% honey solution and $0.1\ \text{M}\ \text{FeCl}_3 \cdot 6\text{H}_2\text{O}$ (98% pure) (1:1) were added to a flask. To this solution, NaOH (99% pure) was added dropwise to set the pH of the solution to 11. The final solution was stirred vigorously for 30 min on a magnetic stirrer until an intense black color was observed. This was an indication of the formation of Fe_2O_3 -NPs. Centrifugation was performed for 40 min at 8000 r.p.m. to separate nanoparticles from other particles in the solution, and then the pellet was washed with water and ethanol three times. An ultra-fine powder of nanoparticles was obtained by keeping the solution in a hot air oven at $80\ ^\circ\text{C}$ for 6–7 h [26].

4.2. Characterization of Honey-Mediated Fe_2O_3 -NPs

The bioactive iron oxide nanomaterials were characterized using a variety of analytical techniques, including UV-Vis spectroscopy, X-ray diffraction analysis (XRD), energy-

dispersive X-ray analysis (EDX), inductively coupled plasma mass spectrometry (ICP-MS), and scanning electron microscopy (SEM). For primary confirmation, UV-Vis spectrophotometry was performed to determine the spectral frequency of Fe₂O₃-NPs in the range of 200–800 nm. Two cleaned cuvettes made of quartz were used for this; one contained water, and the other contained approximately 3 mL of Fe₂O₃-NPs. The pure samples were diluted up to 5 times because using undiluted solutions produced noisy outcomes. After that, the UV-visible range was adjusted between 200 and 800 nm, and peaks were recorded. A BRUKER D8 Discover diffractometer with a 50–500 µm X-ray beam was utilized to study the crystal planes of Fe₂O₃-NPs. This was accomplished by projecting an X-ray beam onto a powdered specimen from the radiation source, which caused reflections to create various diffraction configurations. The precise specimen's crystallographic nature was revealed by these diffraction patterns [58].

The involvement of different elements in the synthesis of Fe₂O₃-NPs was determined by using the EDAX Team at 12.5 kV, 3.84 A, 500×, and 129 eV. For EDX analysis, an electron beam that generated distinct X-rays in the elements of the sample was employed. The detector detected every wavelength of X-rays that the sample emitted. The individual element (the source of the unique X-ray) found in a sample is represented by each X-ray with a wavelength that varies [59]. ICP-MS is an analytical technique that is usually employed to analyze trace elements present in thermally digested biological samples [60]. Before ICP-MS analysis, the sample was thermally digested by aqua regia (1:3 HCl: HNO₃) and diluted. For this, 3 mL HNO₃, 1 mL HCl, and 0.5 g Fe₂O₃-NPs were added to a clean test tube. The solution was heated above 100 °C on a hotplate until the visible mass disappeared (transparent yellow color) from the test tube. The resultant solution was filtered, and 9 mL of deionized water was added to 1 mL of the filtered solution. After that, the determination of trace elements in the digested sample was performed using the ICP-MS Shimadzu model (MY-17320003) at different wavelengths and specific conditions: RF power (1.2), viewing height (8 mm), nebulizer flow (0.7), plasma flow (12), aux flow (1), and make-up flow (0).

The moment of magnetization of prepared Fe₂O₃-NPs was observed using a vibrating sample magnetometer (VSM) at a temperature of 299.0 K with an applied magnetic field of up to 20,000 Oe. The physical properties of honey-mediated Fe₂O₃-NPs were analyzed by scanning electron microscopy (SEM). Real-time pictures of the samples, clarity at the nanometer level of 20 to 100 nm, and a broad traversing zone of nanoparticles are all provided by this methodology [61]. The SEM instrument JSM-6380 with a potential energy of 15 KV and magnification up to 20,000x was used to examine morphological properties (size and shape) of the synthesized Fe₂O₃-NPs.

4.3. Estimation of Antibacterial Potential and MIC

Between October 2021 and December 2021, 30 clinical strains of *K. pneumoniae* were collected from the Pathology laboratory of Nishtar Hospital, Multan, and were named HS-K-1 to HS-K-30. The antibacterial activity of Fe₂O₃-NPs was determined against selected clinical strains of *K. pneumoniae* using the agar well diffusion method. Mueller–Hinton (MH) agar plates were aseptically prepared, and each plate was swabbed with a 0.5 McFarland standard bacterial culture. After drying for 15 min, 3 wells of equal width were generated on each plate using a pipette. The first two wells were loaded with 30 µL of Fe₂O₃-NPs, and the last well was loaded with a diluted honey solution. All plates were incubated at 37 °C overnight. The next day, inhibition zones were measured for each strain, and results were recorded in accordance with CLSI guidelines. By using a sterile 96-well plate, the MIC value of Fe₂O₃-NPs was determined. Aqueous solutions of nanomaterials (20–50 µg/mL) were prepared in sterile broth. In each of the wells, 180 µL of nanoparticle dilution and 20 µL of 0.5 McFarland standard *K. pneumoniae* culture were mixed. After 20 h of incubation at 37 °C, optical density was recorded in an ELISA plate reader (OD₆₂₀). All the analyses were performed in triplicate.

4.4. Synergism with Antibiotics

The Kirby–Bauer disc diffusion method was used to analyze the susceptibility profile of bacteria against three selected antibiotics: ciprofloxacin (CIP-5), gentamicin (CN-10), and cefepime (FEP-30). MH agar plates were prepared, and bacterial lawns were made on agar plates using 0.5 McFarland standard *K. pneumoniae* cultures aseptically. After that, antibiotic discs were impregnated on agar with the help of syringes, and plates were incubated at 37 °C overnight. For determining the synergistic activity of Fe₂O₃-NPs with selected antibiotics, a well diffusion procedure was performed with antibiotics soaked in nanoparticle solution in wells. Subsequent to incubation, zones of inhibition were measured and recorded in accordance with CLSI guidelines for 2022.

4.5. Evaluation of Antioxidant Potential

The antioxidant capacity of Fe₂O₃-NPs was determined using a phosphomolybdenum spectrometric assay. A solution containing 4 mM ammonium molybdate, 0.6 mM sulfuric acid, and 28 mM sodium phosphate was prepared. Different initial concentrations (200–800 µg/mL) of Fe₂O₃-NPs were also prepared. Ascorbic acid (AAE) and honey solution (HON) were included as standards. Following preliminary preparations, 1 mL of sample was mixed with 100 µL of each initial concentration in separate test tubes. Test tubes were incubated in a pre-warmed (95 °C) water bath for an hour and a half. Afterward, the test tubes were removed from the water bath and cooled down to room temperature. Finally, the absorbance of each sample was measured at 695 nm. Total antioxidant capacity (TAC) values were calculated by using the following formula:

$$\text{Total antioxidant capacity (\%)} = (\text{OD}_{\text{control}} - \text{OD}_{\text{sample}}) / \text{OD}_{\text{control}} \times 100 \quad (1)$$

The final results were interpreted as a half-maximal inhibitory concentration (IC₅₀) value.

4.6. Determination of Anti-Inflammatory Potential

For this experiment, an initial solution of 0.2% (*w/v*) bovine serum albumin (BSA) and well as different concentrations of Fe₂O₃-NPs (200–800 µg/mL) were prepared. As standards, ascorbic acid (AAE) and honey solution (HON) were used. Then, 5 mL of BSA solution was mixed with 50 µL of each of the different nanoparticle concentrations in separate test tubes, which were then incubated in a pre-warmed (75 °C) water bath for five minutes. Subsequently, test tubes were removed from the water bath and cooled down to room temperature. Each sample's absorbance was measured at 660 nm in a spectrophotometer. Anti-inflammatory potential values were calculated by using the following formula:

$$\text{Anti-inflammatory capacity \%} = (\text{OD}_{\text{control}} - \text{OD}_{\text{sample}}) / \text{OD}_{\text{control}} \times 100 \quad (2)$$

The final results were interpreted as a half-maximal inhibitory concentration (IC₅₀) value.

5. Conclusions

In conclusion, nanotechnology has become a rapidly expanding branch of science in recent years due to widespread applications in the environment, industries, electronics, and medicine. Organic honey was used in the present investigation for the green production of nanoparticles based on iron oxide, representing a safe, sustainable, nontoxic, easily accessible, and economical approach. The phytochemical constituents present on the particle surface lower the chances of clumping, making the Fe₂O₃-NPs fabricated in the present study more stable than chemically produced nanoparticles. Additionally, they have the advantage of being simpler to separate as compared to other metal oxide nanoparticles, which call for extremely labor-intensive centrifugation. Furthermore, these nanoparticles exhibited considerable antibacterial, antioxidant, and anti-inflammatory actions against clinically isolated *K. pneumoniae* strains. Together, this makes them candidates for promising antimicrobial agents with prospective biomedical applications.

Author Contributions: Conceptualization, H.S., M.J. and I.A.; methodology, M.J. and A.Z.N.; software, S.N.U.S.B., A.Z.N. and M.J.; validation, S.N.U.S.B.; formal analysis, H.S., A.A.S. and A.D.C.; investigation, A.Z.N. and M.J.; resources, M.F.; data curation, A.A.S., A.Z.N. and A.D.C.; writing—original draft preparation, H.S. and I.A.; writing—review and editing, I.A., M.A., M.F., S.J.G. and M.N.B.J.; visualization, M.N.B.J. and M.F.; supervision, I.A.; project administration, I.A., M.N.B.J. and A.A.S.; funding acquisition, S.J.G. All authors have read and agreed to the published version of the manuscript.

Funding: This study was funded by the Princess Nourah bint Abdulrahman University Researchers Supporting Project number (PNURSP2023R108), Princess Nourah bint Abdulrahman University, Riyadh, Saudi Arabia.

Institutional Review Board Statement: Not applicable.

Informed Consent Statement: Not applicable.

Data Availability Statement: Data will be available from authors on reasonable request.

Acknowledgments: This research project was supported by the Princess Nourah bint Abdulrahman University Researchers Supporting Project number (PNURSP2023R108), Princess Nourah bint Abdulrahman University, Riyadh, Saudi Arabia.

Conflicts of Interest: The authors have no conflict of interest to declare.

Sample Availability: Not available.

References

- Gopu, M.; Kumar, P.; Selvakumar, T.; Senthilkumar, B.; Sudhakar, C.; Govarthanan, M.; Selvam, K. Green biomimetic silver nanoparticles utilizing the red algae *Amphiroa rigida* and its potent antibacterial, cytotoxicity and larvicidal efficiency. *Bioprocess Biosyst. Eng.* **2021**, *44*, 217–223. [\[CrossRef\]](#) [\[PubMed\]](#)
- Shah, A.A.; Bhatti, M.A.; Tahira, A.; Chandio, A.D.; Channa, I.A.; Sahito, A.G.; Chalanger, E.; Willander, M.; Nur, O.; Ibupoto, Z.H. Facile synthesis of copper doped ZnO nanorods for the efficient photo degradation of methylene blue and methyl orange. *Ceram. Int.* **2020**, *46*, 9997–10005. [\[CrossRef\]](#)
- Üstün, E.; Önbaşı, S.C.; Çelik, S.K.; Ayvaz, M.Ç.; Şahin, N. Green synthesis of iron oxide nanoparticles by using *Ficus carica* leaf extract and its antioxidant activity. *Biointerface Res. Appl. Chem.* **2022**, *2021*, 2108–2116.
- Neupane, B.P.; Chaudhary, D.; Paudel, S.; Timsina, S.; Chapagain, B.; Jamarkattel, N.; Tiwari, B.R. Himalayan honey loaded iron oxide nanoparticles: Synthesis, characterization and study of antioxidant and antimicrobial activities. *Int. J. Nanomed.* **2019**, *14*, 3533. [\[CrossRef\]](#) [\[PubMed\]](#)
- Rostamizadeh, E.; Iranbakhsh, A.; Majd, A.; Arbabian, S.; Mehregan, I. Green synthesis of Fe₂O₃ nanoparticles using fruit extract of *Cornus mas* L. and its growth-promoting roles in Barley. *J. Nanostructure Chem.* **2020**, *10*, 125–130. [\[CrossRef\]](#)
- Ali, I.; Pan, Y.; Jamil, Y.; Chen, J.; Shah, A.A.; Imran, M.; Alvi, U.; Nasir, N.; Shen, Z. Hybrid Au/Co nanoparticles: Laser-assisted synthesis and applications in magnetic hyperthermia. *Phys. B: Condens. Matter* **2023**, *657*, 414773. [\[CrossRef\]](#)
- Ali, I.; Pan, Y.; Jamil, Y.; Shah, A.A.; Amir, M.; Al Islam, S.; Fazal, Y.; Chen, J.; Shen, Z. Comparison of copper-based Cu-Ni and Cu-Fe nanoparticles synthesized via laser ablation for magnetic hyperthermia and antibacterial applications. *Phys. B Condens. Matter* **2023**, *650*, 414503. [\[CrossRef\]](#)
- Tufani, A.; Qureshi, A.; Niazi, J.H. Iron oxide nanoparticles based magnetic luminescent quantum dots (MQDs) synthesis and biomedical/biological applications: A review. *Mater. Sci. Eng. C* **2021**, *118*, 111545. [\[CrossRef\]](#)
- AlMatar, M.; Makky, E.A.; Var, I.; Koksall, F. The role of nanoparticles in the inhibition of multidrug-resistant bacteria and biofilms. *Curr. Drug Deliv.* **2018**, *15*, 470–484. [\[CrossRef\]](#)
- Gudkov, S.V.; Burmistrov, D.E.; Serov, D.A.; Rebezov, M.B.; Semenova, A.A.; Lisitsyn, A.B. Do iron oxide nanoparticles have significant antibacterial properties? *Antibiotics* **2021**, *10*, 884. [\[CrossRef\]](#) [\[PubMed\]](#)
- Baimler, I.V.; Lisitsyn, A.B.; Gudkov, S.V. Water decomposition occurring during laser breakdown of aqueous solutions containing individual gold, zirconium, molybdenum, iron or nickel nanoparticles. *Front. Phys.* **2020**, *8*, 620938. [\[CrossRef\]](#)
- Lozhkomoev, A.; Pervikov, A.; Kazantsev, S.; Sharipova, A.; Rodkevich, N.; Toropkov, N.; Lerner, M. Synthesis of Fe/Fe₃O₄ core-shell nanoparticles by electrical explosion of the iron wire in an oxygen-containing atmosphere. *J. Nanoparticle Res.* **2021**, *23*, 73. [\[CrossRef\]](#)
- Stolyar, S.; Krasitskaya, V.; Frank, L.; Yaroslavl'tsev, R.; Chekanova, L.; Gerasimova, Y.; Velikanov, D. Polysaccharide-coated iron oxide nanoparticles: Synthesis, properties, surface modification. *Mater. Lett.* **2021**, *284*, 128920. [\[CrossRef\]](#)
- Tyurikova, I.A.; Alexandrov, S.E.; Tyurikov, K.S.; Kirilenko, D.A.; Speshilova, A.B.; Shakhmin, A.L. Fast and controllable synthesis of core-shell Fe₃O₄-C nanoparticles by aerosol CVD. *ACS Omega* **2020**, *5*, 8146–8150. [\[CrossRef\]](#) [\[PubMed\]](#)
- Nagajyothi, P.; Pandurangan, M.; Kim, D.H.; Sreekanth, T.; Shim, J. Green synthesis of iron oxide nanoparticles and their catalytic and in vitro anticancer activities. *J. Clust. Sci.* **2017**, *28*, 245–257. [\[CrossRef\]](#)

16. Patil, S.P.; Chaudhari, R.Y.; Nemade, M.S. *Azadirachta indica* leaves mediated green synthesis of metal oxide nanoparticles: A review. *Talanta Open* **2022**, *5*, 100083. [\[CrossRef\]](#)
17. Rizvi, M.; Bhatia, T.; Gupta, R. Green & sustainable synthetic route of obtaining iron oxide nanoparticles using *Hylocereus undantus* (pitaya or dragon fruit). *Mater. Today Proc.* **2022**, *50*, 1100–1106.
18. Buarki, F.; AbuHassan, H.; Al Hannan, F.; Henari, F. Green Synthesis of Iron Oxide Nanoparticles Using *Hibiscus rosa sinensis* Flowers and Their Antibacterial Activity. *J. Nanotechnol.* **2022**, *2022*, 5474645. [\[CrossRef\]](#)
19. Salgado, P.; Márquez, K.; Rubilar, O.; Contreras, D.; Vidal, G. The effect of phenolic compounds on the green synthesis of iron nanoparticles (Fe₃O₄-NPs) with photocatalytic activity. *Appl. Nanosci.* **2019**, *9*, 371–385. [\[CrossRef\]](#)
20. Abeska, Y.Y.; Cavas, L. Artificial neural network modeling of green synthesis of silver nanoparticles by honey. *Neural Netw. World* **2022**, *32*, 1. [\[CrossRef\]](#)
21. Mandey, F.; Zakir, M.; Noor, A. Utilization of polyfloral honey in the synthesis of gold nanoparticles and evaluation of its potency as an antibacterial against *S. aureus* and *E. coli*. *J. Phys. Conf. Ser.* **2019**, *1341*, 032007. [\[CrossRef\]](#)
22. Keskin, M.; Kaya, G.; Keskin, S. Nanotechnology in Honey: Future and Perspectives Honey as Nanoparticles. In *Nanotechnology in Functional Foods*; Scrivener Publishing LLC: Beverly, MA, United States, 2022; pp. 87–101.
23. Sharmila, M.; Mani, R.J.; Parvathiraja, C.; Kader, S.M.A.; Siddiqui, M.R.; Wabaidur, S.M.; Lai, W.C. Photocatalytic Dye Degradation and Bio-Insights of Honey-Produced α -Fe₂O₃ Nanoparticles. *Water* **2022**, *14*, 2301. [\[CrossRef\]](#)
24. Haris, M.; Fatima, N.; Iqbal, J.; Chalgham, W.; Mumtaz, A.S.; El-Sheikh, M.A.; Tavafoghi, M. *Oscillatoria limnetica* Mediated Green Synthesis of Iron Oxide (Fe₂O₃) Nanoparticles and Their Diverse In Vitro Bioactivities. *Molecules* **2023**, *28*, 2091. [\[CrossRef\]](#)
25. Awais, S.; Munir, H.; Najeeb, J.; Anjum, F.; Naseem, K.; Kausar, N.; Najeeb, N. Green synthesis of iron oxide nanoparticles using *Bombax malabaricum* for antioxidant, antimicrobial and photocatalytic applications. *J. Clean. Prod.* **2023**, *406*, 136916. [\[CrossRef\]](#)
26. Bhuiyan, M.S.H.; Miah, M.Y.; Paul, S.C.; Aka, T.D.; Saha, O.; Rahaman, M.M.; Ashaduzzaman, M. Green synthesis of iron oxide nanoparticle using *Carica papaya* leaf extract: Application for photocatalytic degradation of remazol yellow RR dye and antibacterial activity. *Heliyo* **2020**, *6*, e04603. [\[CrossRef\]](#)
27. Hammad, E.N.; Salem, S.S.; Mohamed, A.A.; El-Dougdoug, W. Environmental impacts of ecofriendly iron oxide nanoparticles on dyes removal and antibacterial activity. *Appl. Biochem. Biotechnol.* **2022**, *194*, 6053–6067. [\[CrossRef\]](#) [\[PubMed\]](#)
28. Lee, C.-R.; Lee, J.H.; Park, K.S.; Jeon, J.H.; Kim, Y.B.; Cha, C.J.; Lee, S.H. Antimicrobial resistance of hypervirulent *Klebsiella pneumoniae*: Epidemiology, hypervirulence-associated determinants, and resistance mechanisms. *Front. Cell. Infect. Microbiol.* **2017**, *7*, 483. [\[CrossRef\]](#)
29. Falcone, M.; Tiseo, G.; Arcari, G.; Leonildi, A.; Giordano, C.; Tempini, S.; Carattoli, A. Spread of hypervirulent multidrug-resistant ST147 *Klebsiella pneumoniae* in patients with severe COVID-19: An observational study from Italy, 2020–21. *J. Antimicrob. Chemother.* **2022**, *77*, 1140–1145. [\[CrossRef\]](#)
30. Kaur, K.; Sidhu, A.K. Green synthesis: An eco-friendly route for the synthesis of iron oxide nanoparticles. *Front. Nanotechnol.* **2021**, *3*, 655062.
31. Bahari, N.; Hashim, N.; Abdan, K.; Md Akim, A.; Maringgal, B.; Al-Shdifat, L. Role of Honey as a Bifunctional Reducing and Capping/Stabilizing Agent: Application for Silver and Zinc Oxide Nanoparticles. *Nanomaterials* **2023**, *13*, 1244. [\[CrossRef\]](#)
32. Abdel-Raouf, N.; Al-Enazi, N.M.; Ibraheem, I.B.M.; Alharbi, R.M.; Alkhulaifi, M.M. Biosynthesis of silver nanoparticles by using of the marine brown alga *Padina pavonia* and their characterization. *Saudi J. Biol. Sci.* **2019**, *26*, 1207–1215. [\[CrossRef\]](#) [\[PubMed\]](#)
33. Azadi, F.; Karimi-Jashni, A.; Zerafat, M.M. Green synthesis and optimization of nano-magnetite using *Persicaria bistorta* root extract and its application for rosewater distillation wastewater treatment. *Ecotoxicol. Environ. Saf.* **2018**, *165*, 467–475. [\[CrossRef\]](#)
34. Qayoom, M.; Shah, K.A.; Pandit, A.H.; Firdous, A.; Dar, G.N. Dielectric and electrical studies on iron oxide (α -Fe₂O₃) nanoparticles synthesized by modified solution combustion reaction for microwave applications. *J. Electroceramics* **2020**, *45*, 7–14. [\[CrossRef\]](#)
35. Biswas, A.; Vanlalveni, C.; Lalfakzuala, R.; Nath, S.; Rokhum, L. *Mikania mikrantha* leaf extract mediated biogenic synthesis of magnetic iron oxide nanoparticles: Characterization and its antimicrobial activity study. *Mater. Today Proc.* **2021**, *42*, 1366–1373. [\[CrossRef\]](#)
36. Menazea, A.; Ahmed, M. Silver and copper oxide nanoparticles-decorated graphene oxide via pulsed laser ablation technique: Preparation, characterization, and photoactivated antibacterial activity. *Nano-Struct. Nano-Objects* **2020**, *22*, 100464. [\[CrossRef\]](#)
37. Qasim, S.; Zafar, A.; Saif, M.S.; Ali, Z.; Nazar, M.; Waqas, M.; Iqbal, F. Green synthesis of iron oxide nanorods using *Withania coagulans* extract improved photocatalytic degradation and antimicrobial activity. *J. Photochem. Photobiol. B Biol.* **2020**, *204*, 111784. [\[CrossRef\]](#) [\[PubMed\]](#)
38. Beheshtkhoo, N.; Kouhbanani, M.A.J.; Savardashtaki, A.; Amani, A.M.; Taghizadeh, S. Green synthesis of iron oxide nanoparticles by aqueous leaf extract of *Daphne mezereum* as a novel dye removing material. *Appl. Phys. A* **2018**, *124*, 363. [\[CrossRef\]](#)
39. Vasantharaj, S.; Sathiyavimal, S.; Senthilkumar, P.; LewisOscar, F.; Pugazhendhi, A. Biosynthesis of iron oxide nanoparticles using leaf extract of *Ruellia tuberosa*: Antimicrobial properties and their applications in photocatalytic degradation. *J. Photochem. Photobiol. B Biol.* **2019**, *192*, 74–82. [\[CrossRef\]](#)
40. Roychoudhury, P.; Golubeva, A.; Dabek, P.; Pryshchepa, O.; Sagandykova, G.; Pomastowski, P.; Buszewski, B. Study on biogenic spindle-shaped iron-oxide nanoparticles by *Pseudostaurosira trainorii* in field of laser desorption/ionization applications. *Int. J. Mol. Sci.* **2022**, *23*, 11713. [\[CrossRef\]](#)
41. Teja, A.S.; Koh, P.-Y. Synthesis, properties, and applications of magnetic iron oxide nanoparticles. *Prog. Cryst. Growth Charact. Mater.* **2009**, *55*, 22–45. [\[CrossRef\]](#)

42. Aida, M.; Alonizan, N.; Zarrad, B.; Hjiri, M. Green synthesis of iron oxide nanoparticles using *Hibiscus* plant extract. *J. Taibah Univ. Sci.* **2023**, *17*, 2221827. [\[CrossRef\]](#)
43. Karade, V.; Parit, S.; Dawkar, V.; Devan, R.; Choudhary, R.; Kedge, V.; Pawar, N.; Kim, J.; Chougale, A. A green approach for the synthesis of α -Fe₂O₃ nanoparticles from *Gardenia resinifera* plant and its in vitro hyperthermia application. *Heliyon* **2019**, *5*, e02044. [\[CrossRef\]](#)
44. Xia, C.; Hu, C.; Xiong, Y.; Wang, N. Synthesis of α -Fe₂O₃ hexagons and their magnetic properties. *J. Alloy. Compd.* **2009**, *480*, 970–973. [\[CrossRef\]](#)
45. Miri, A.; Najafzadeh, H.; Darroudi, M.; Miri, M.J.; Kouhbanani, M.A.J.; Sarani, M. Iron oxide nanoparticles: Biosynthesis, magnetic behavior, cytotoxic effect. *ChemistryOpen* **2021**, *10*, 327–333. [\[CrossRef\]](#)
46. Salama, A.; Abedin, R.; Elwakeel, K. Influences of greenly synthesized iron oxide nanoparticles on the bioremediation of dairy effluent using selected microbial isolates. *Int. J. Environ. Sci. Technol.* **2022**, *19*, 7019–7030. [\[CrossRef\]](#)
47. Ahmad, W.; Kumar Jaiswal, K.; Amjad, M. Euphorbia herita leaf extract as a reducing agent in a facile green synthesis of iron oxide nanoparticles and antimicrobial activity evaluation. *Inorg. Nano-Met. Chem.* **2021**, *51*, 1147–1154. [\[CrossRef\]](#)
48. Kirdat, P.; Dandge, P.; Hagwane, R.; Nikam, A.; Mahadik, S.; Jirange, S. Synthesis and characterization of ginger (*Z. officinale*) extract mediated iron oxide nanoparticles and its antibacterial activity. *Mater. Today Proc.* **2021**, *43*, 2826–2831. [\[CrossRef\]](#)
49. Awwad, A.M.; Amer, M.W.; Salem, N.M.; Abdeen, A.O. Green synthesis of zinc oxide nanoparticles (ZnO-NPs) using *Ailanthus altissima* fruit extracts and antibacterial activity. *Chem. Int.* **2020**, *6*, 151–159.
50. Noreen, S.; Mustafa, G.; Ibrahim, S.M.; Naz, S.; Iqbal, M.; Yaseen, M.; Nisar, J. Iron oxide (Fe₂O₃) prepared via green route and adsorption efficiency evaluation for an anionic dye: Kinetics, isotherms and thermodynamics studies. *J. Mater. Res. Technol.* **2020**, *9*, 4206–4217. [\[CrossRef\]](#)
51. Ahmad, W.; Jaiswal, K.K.; Soni, S. Green synthesis of titanium dioxide (TiO₂) nanoparticles by using *Mentha arvensis* leaves extract and its antimicrobial properties. *Inorg. Nano-Met. Chem.* **2020**, *50*, 1032–1038. [\[CrossRef\]](#)
52. Awwad, A.M.; Salem, N.M.; Aqarbeh, M.M.; Abdulaziz, F.M. Green synthesis, characterization of silver sulfide nanoparticles and antibacterial activity evaluation. *Chem. Int.* **2020**, *6*, 42–48.
53. Abo-Shama, U.H.; El-Gendy, H.; Mousa, W.S.; Hamouda, R.A.; Yousuf, W.E.; Hetta, H.F.; Abdeen, E.E. Synergistic and antagonistic effects of metal nanoparticles in combination with antibiotics against some reference strains of pathogenic microorganisms. *Infect. Drug Resist.* **2020**, *13*, 351. [\[CrossRef\]](#)
54. Bouafia, A.; Laouini, S.E.; Khelef, A.; Tedjani, M.L.; Guemari, F. Effect of ferric chloride concentration on the type of magnetite (Fe₃O₄) nanoparticles biosynthesized by aqueous leaves extract of artemisia and assessment of their antioxidant activities. *J. Clust. Sci.* **2021**, *32*, 1033–1041. [\[CrossRef\]](#)
55. Mohamed, N.; Hessen, O.E.; Mohammed, H.S. Thermal stability, paramagnetic properties, morphology and antioxidant activity of iron oxide nanoparticles synthesized by chemical and green methods. *Inorg. Chem. Commun.* **2021**, *128*, 108572. [\[CrossRef\]](#)
56. Periakaruppan, R.; Chen, X.; Thangaraj, K.; Jeyaraj, A.; Nguyen, H.H.; Yu, Y.; Li, X. Utilization of tea resources with the production of superparamagnetic biogenic iron oxide nanoparticles and an assessment of their antioxidant activities. *J. Clean. Prod.* **2021**, *278*, 123962. [\[CrossRef\]](#)
57. Yadav, E.; Yadav, P.; Verma, A. Amelioration of full thickness dermal wounds by topical application of biofabricated zinc oxide and iron oxide nano-ointment in albino Wistar rats. *J. Drug Deliv. Sci. Technol.* **2021**, *66*, 102833. [\[CrossRef\]](#)
58. Raval, N.; Maheshwari, R.; Kalyane, D.; Youngren-Ortiz, S.R.; Chougale, M.B.; Tekade, R.K. Importance of physicochemical characterization of nanoparticles in pharmaceutical product development. In *Basic Fundamentals of Drug Delivery*; Elsevier: Amsterdam, The Netherlands, 2019; pp. 369–400.
59. Scimeca, M.; Bischetti, S.; Lamsira, H.K.; Bonfiglio, R.; Bonanno, E. Energy Dispersive X-ray (EDX) microanalysis: A powerful tool in biomedical research and diagnosis. *Eur. J. Histochem. EJH* **2018**, *62*, 2841. [\[CrossRef\]](#) [\[PubMed\]](#)
60. Wilschefschi, S.C.; Baxter, M.R. Inductively coupled plasma mass spectrometry: Introduction to analytical aspects. *Clin. Biochem. Rev.* **2019**, *40*, 115. [\[CrossRef\]](#)
61. Qu, J.; Liu, X. Recent advances on SEM-based in situ multiphysical characterization of nanomaterials. *Scanning* **2021**, *2021*, 4426254. [\[CrossRef\]](#)

Disclaimer/Publisher's Note: The statements, opinions and data contained in all publications are solely those of the individual author(s) and contributor(s) and not of MDPI and/or the editor(s). MDPI and/or the editor(s) disclaim responsibility for any injury to people or property resulting from any ideas, methods, instructions or products referred to in the content.